

# Infrastructure adaptation and emergence of loops in network routing with time-dependent loads

Alessandro Lonardi<sup>1</sup>, Enrico Facca<sup>2</sup>, Mario Putti<sup>3</sup> and Caterina De Bacco<sup>1</sup>

<sup>1</sup>Max Planck Institute for Intelligent Systems, Cyber Valley, Tübingen 72076, Germany

<sup>2</sup>Univ. Lille, Inria, CNRS, UMR 8524 - Laboratoire Paul Painlevé, F-59000 Lille, France

<sup>3</sup>Department of Mathematics “Tullio Levi-Civita”, University of Padua, Via Trieste 63, Padua, Italy

**Abstract.** Network routing approaches are widely used to study the evolution in time of self-adapting systems. However, few advances have been made for problems where adaptation is governed by time-dependent inputs. In this work, we study a dynamical systems where the edge conductivities—capacities—of a network are regulated by time-varying mass loads injected on nodes. Motivated by empirical observations, we assume that conductivities adapt slowly with respect to the characteristic time of the loads. Furthermore, assuming the loads to be periodic, we derive a new dynamics where the evolution of the system is governed by a matrix obtained with the Fourier coefficients of the input loads. Remarkably, we find a sufficient condition on these coefficients that determines when the resulting network topologies are trees. We show an example of this on the Bordeaux bus network where we tune the input loads to interpolate between loopy and tree topologies. We validate our model on several synthetic networks and provide an expression for long-time solutions of the original conductivities, supported by numerical observations and analytical arguments.

*Keywords:* optimal transport, network routing, network design, loops emergence, transportation network

## 1. Introduction

Optimized transport of resources is a pivotal contributing factor in determining the structural evolution of real-world networks. Archetypes for self-organizing systems that ramify into networks in order to optimize energy expenditure rates are xylem conduits in leaves [1–4], river basins [5–9], and slime molds [10–19]. These formations are not only restricted to the natural realm but can also be generated by anthropogenic processes. A prominent example is that of transportation networks such as railway and metro systems, that are designed to jointly optimize traffic overload and infrastructural cost [20–22].

Typically, optimal transport of mass in networks is set as a minimization problem where resources moving through the edges have to satisfy a set of constraints, e.g., conservation of mass, while minimizing a suitable transportation cost [1, 3, 19, 23–30]. Several efficient methods have been proposed to solve this problem. A popular approach is that of message-passing algorithms [31], where sources of mass are matched in sender-receiver pairs, and messages encode mass transfer between them [22, 32–36]. Promising results have also been obtained with optimal transport theory [2, 15, 20, 27, 37–42]—the approach we consider in this work. The general idea behind this method is to describe the transport of mass as a process being regulated by capacities on edges, quantities determined using a dynamical system that couples them with fluxes of mass allocated on edges.

Despite their usage in modeling transportation problems across domains, a common drawback of all these methods is to consider only stationary loads, i.e. resources that are injected and travel through the network do not change with time. This assumption may not be valid in certain scenarios. For instance, blood vessels are known for adapting their structure continuously to meet changing metabolic demands [25, 43–45]. Similarly, passengers in transportation systems enter stations with hourly, weekly, and seasonal time-varying rates [46]. A viable approach to model these systems is to control the network evolution considering an ensemble average of the stress generated by the loads [24, 25, 37]. This relies on assuming stationary loads on nodes but with their positions varied stochastically. The ensemble average over the loads' locations is then computed as a proxy of a system with loads of fixed locations but time-varying amounts. This technique has also been employed to study networks resilience to edge cutting [3], or for routing problems with spatially correlated loads [2].

Remarkably, adding stochasticity in the loads may lead to the emergence of loops in the resulting optimal networks topologies [2, 3, 24, 25, 37]. This result is complementary to the hierarchical formation of trees since loops provide alternative routes to accommodate fluctuations or guarantee robustness against broken links. Recently, loops formation has also been observed in multicommodity setups [27, 28], where the loads are deterministic inputs of the problem. In this case, loops generation is a consequence of having different types of mass—commodities—interacting in a unique shared infrastructure.

In all these works, however, the time-varying character of the transport network loads is neglected because the main problem variables are taken on average. Instead, here we develop a model that considers the explicit time dependence of the mass inflows and investigate, both analytically and numerically, the long-term behavior of time-varying transport networks.

In particular, we generalize the routing problem in Facca *et al.* [41] by considering periodic mass loads on nodes. We postulate an analytical relationship connecting

physical quantities as the edge conductivities (or capacities) and the coefficients of the Fourier series expansion of the loads. We then define a new dynamics that rapidly converges to the long-run average solutions of the original dynamics. Remarkably, we find that the Fourier decomposition of the loads yields a sufficient condition to determine whether the resulting optimal networks will contain loops or have a tree-like structure. Performing a numerical validation of our dynamics on synthetic networks we are also able to provide an analytical expression for the long-run conductivities.

Precisely, we find that the conductivities start oscillating around constant values at large time scales, at certain frequencies that can be expressed in terms of those of the input loads. Furthermore, we define a valid Lyapunov functional for our dynamical formulation, allowing us to interpret stationary topologies as optimal networks, i.e. structures minimizing the global cost to build the graph. Lastly, we examine a case study with loads that are the sum of decoupled harmonic oscillators, finding that the condition on the Fourier coefficients can be equivalently reformulated in terms of the loads' amplitudes and phases. We numerically investigate this last setup applying it to the real dataset of the Bordeaux bus network.

## 2. Time-varying loads in routing optimization on networks

Consider a network  $G(V, E)$  with nodes  $v \in V$  and edges  $e \in E$ , each of length  $\ell_e > 0$ . The orientation of the edges is conventionally assigned by the signed incidence matrix of the network, with entries  $B_{ve} = \pm 1$  if node  $v$  is the tail or the head of edge  $e$ , and  $B_{ve} = 0$  otherwise. We consider a routing optimization problem on  $G$  setting time-varying mass loads  $S(t) = \{S_v(t)\}_v$  on nodes, with  $S_v(t) \in \mathbb{R}$  being the amount of mass either injected in ( $S_v(t) > 0$ ) or extracted from ( $S_v(t) < 0$ ) node  $v$ . This allows us to write Kirchoff's conservation law as

$$\sum_u L_{vu}(\mu) p_u(t) = S_v(t) \quad \forall v \in V, \forall t \geq 0, \quad (1)$$

where  $\mu = \{\mu_e\}_e \geq 0$  are the edge conductivities,  $p(t) = \{p_v(t)\}_v$  are pressure potentials on nodes and  $L_{vu}(\mu) := \sum_e B_{ve}(\mu_e/\ell_e)B_{ue}$  are the entries of the weighted Laplacian of the network [47]. The conductivities  $\mu$  can be interpreted as the capacities that the edges should have to successfully allocate the mass loads acting on the nodes, thus we can consider them proportional to edges sizes.

We propose a model in which the forcings  $S(t)$  dictate the time evolution of the conductivities by means of a feedback dynamics. In particular, we couple (1) with the system of ODEs

$$\frac{d\mu_e(t)}{dt} = \frac{F_e^2(t)}{\mu_e^\gamma(t)} - \mu_e(t) \quad \forall e \in E \quad (2)$$

$$\mu_e(0) = m_e \quad \forall e \in E, \quad (3)$$

with  $m_e > 0$  initial values of the conductivities, and where for a solution trajectory  $\mu(t)$ , we define the fluxes entries  $F_e(t) \equiv F_e(\mu(t), S(t)) := \mu_e(t)(p_u(t) - p_v(t))/\ell_e$  for  $e = (u, v)$ , with  $p_v(t) \equiv p_v(\mu(t), S(t)) := \sum_u L_{vu}^\dagger(\mu(t))S_u(t)$  solution of (1), where  $L^\dagger$  denotes the Laplacian pseudo-inverse. We assume that the system is isolated, i.e.  $\sum_v S_v(t) = 0, \forall t \geq 0$ , so that  $p(t)$  is a well-defined potential [47].

The exponent  $0 < \gamma < 2$  tunes between different transportation mechanisms [27, 38, 41]. The case  $\gamma < 1$  encourages mass consolidation on few edges,  $\gamma = 1$  is shortest-path like, while  $1 < \gamma < 2$  penalizes traffic congestion.

### 3. Model construction

#### 3.1. Slow adaptation of conductivities

In several biological systems the adaptation time of organisms is much slower (weeks) than the characteristic time of the mass injected in the system (seconds) [25, 43–45]. In order to describe these organisms, a common approach is that of approximating the fast time-varying input loads with combinations of open and closed switch-like nodes with constant inflows, and then to assume that the conductivities are regulated by an ensemble average of the pressures over different states of the loads [3, 24, 25, 37].

Instead, here we want to model the evolution of these slow adapting conductivities taking in account the time dependence of the loads. We formalize this hypothesis by assuming: (i) the existence of a slow time scale  $\tau$ , with  $\tau = Kt$  and  $K \gg 1$ ; (ii) that in a fixed time window  $\Delta$ , small with respect to the slow variable  $\tau$  but large with respect to the time  $t$ , the following holds

$$\hat{\mu}_e(\tau + t') \approx \hat{\mu}_e(\tau) \quad \forall e \in E, \forall t' \in [0, \Delta) \text{ and } \forall \tau \geq 0, \quad (4)$$

for some conductivities  $\hat{\mu} = \{\hat{\mu}_e\}_e \geq 0$ , with natural time of evolution being  $\tau$ . Example time scales are seconds for  $t$ , days for  $\Delta$  and months for  $\tau$ . Such distinction between different natural time scales is observed in studying the interplay of rivers and tide loads in coastal deltas formation [9], where the assumption is that tides cycle much faster than the river channel adaptation, a distinction analogous to that between our  $t$  and  $\tau$ . Finally, we assume (iii) that the evolution in  $\tau$  of  $\hat{\mu}$  is determined by the time integral average of the squared mass loads. Assumptions (i), (ii) and (iii) together lead to the definition:

$$\hat{\Phi}_e(\hat{\mu}, \tau) := \frac{\hat{\mu}_e^{2-\gamma}}{\ell_e^2} \sum_{uv} A_{eu}(\hat{\mu}) A_{ev}(\hat{\mu}) \frac{1}{\Delta} \int_{\tau}^{\tau+\Delta} S_u(t) S_v(t) dt - \hat{\mu}_e \quad \forall e \in E, \forall \tau \geq 0, \quad (5)$$

where we introduced  $A_{ev}(\hat{\mu}) := \sum_u B_{eu} L_{vu}^\dagger(\hat{\mu})$ ,  $\forall e \in E, \forall v \in V$ . The functional  $\hat{\Phi}$  is the natural approximation of the right hand side of (2), as shown in Appendix A. Now, a trajectory  $\hat{\mu}(\tau)$  is defined as a solution of the dynamics

$$\frac{d\hat{\mu}_e(\tau)}{d\tau} = \hat{\Phi}_e(\hat{\mu}(\tau), \tau) \quad (6)$$

$$\hat{\mu}_e(0) = \hat{m}_e, \quad (7)$$

valid  $\forall e \in E$ , with  $\hat{m}_e > 0$  initial conditions.

In general,  $\hat{\Phi}$  is difficult to manipulate as the loads  $S(t)$  may assume any arbitrary expression, possibly preventing the exact computation of the time integrals. For this reason, we investigate its behavior for a particular class of functions  $S(t)$  that allows for analytical tractability.

#### 3.2. Periodicity of the loads

We consider periodic loads  $S(t)$ , with period  $T$  small with respect to the fixed integration window  $\Delta$ :

$$S_v(t + T) = S_v(t), \quad T/\Delta \ll 1 \quad \forall v \in V, \forall t \geq 0. \quad (8)$$

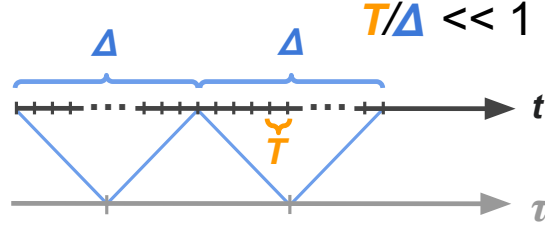


**Figure 1.** Schematic representation of the different time variables. The two arrows denote time scales  $t$  and  $\tau$ . The time windows  $\Delta$ , large with respect to  $t$ , are denoted with blue curved brackets and the fast period  $T$  in orange. Each window  $\Delta$  along which we integrate the dynamics (1)-(3) contains a large number of periods  $T$ .

This allows to express each  $S_v(t)$  using its Fourier series representation  $S_v(t) = \sum_{n_v \in \mathbb{Z}} c_v^{n_v} \exp(i\omega n_v t)$ , with  $\omega = 2\pi/T$ . Substituting this into (5) yields

$$\frac{1}{\Delta} \int_{\tau}^{\tau+\Delta} S_u(t) S_v(t) dt = C_{uv} + \mathcal{O}(\Delta) \quad \forall u, v \in V, \forall \tau \geq 0, \quad (9)$$

where we define the matrix  $C$ , with entries  $C_{uv} := \sum_{n_v} (c_u^{n_v})^* c_v^{n_v}$ ,  $\forall u, v \in V$ . Here,  $c^*$  denotes the complex conjugation of  $c$ . The term  $\mathcal{O}(\Delta)$  contains all negligible contributions  $\varepsilon$ , decaying as  $\varepsilon/\Delta \rightarrow 0$  for  $\Delta \rightarrow +\infty$ . For a detailed derivation of this result one can refer to [Appendix B](#).

### 3.3. Periodic-loads dynamics

Combining (5) and (9) we can build a dynamics for some new conductivities  $\bar{\mu} = \{\bar{\mu}_e\}_e \geq 0$ , which evolve in the slow time scale  $\tau$ . Precisely, we ignore negligible contributions in (9) and define

$$\frac{d\bar{\mu}_e(\tau)}{d\tau} = \bar{\Phi}_e(\bar{\mu}_e(\tau)) \quad (10)$$

$$\bar{\mu}_e(0) = \bar{m}_e, \quad (11)$$

valid  $\forall e \in E$  and with  $\bar{m}_e > 0$  initial condition. The right hand side of (10) is such that  $\hat{\Phi} \simeq \bar{\Phi}$  for  $\Delta \gg 1$ , and reads

$$\bar{\Phi}_e(\bar{\mu}) := \frac{\bar{\mu}_e^{2-\gamma}}{\ell_e^2} \sum_{uv} A_{eu}(\bar{\mu}) A_{ev}(\bar{\mu}) C_{uv} - \bar{\mu}_e \quad \forall e \in E. \quad (12)$$

An important point is that the problem (10)-(11) is *not* equivalent to the dynamics (1)-(3) with each  $S_v(t)$  integrated over  $T$ . The latter case would imply that  $C_{vu}$  had the form  $C_{vu} = \tilde{S}_u \tilde{S}_v$ , where  $\tilde{S}_v$  is the integral of  $S_v(t)$  over the period. This is only a particular case of the dynamics in (10). Noticeably, in this case the condition  $\text{rank}(C) = 1$  holds, i.e. since  $C$  is symmetric, it exists a vector  $y \in \mathbb{R}^{|V|}$  such that  $C_{uv} = y_u y_v$ ,  $\forall u, v \in V$ . This is a sufficient condition for (10)-(11) to return a loop-less network at convergence (see [Appendix C](#) for a proof), and confirms previous results observed for constant loads [23,26,29]. However, this condition does not hold generally

for any arbitrary choice of the loads, as  $C$  may have a more general expression in that case, in particular  $\text{rank}(C) > 1$ . Moreover, the case of constant loads is not the only one where  $\text{rank}(C) = 1$ . We provide an example of this in [Section 5.2](#), where we explore the case of each  $S_v(t)$  being the sum of a finite number of harmonic oscillators.

#### 4. Characterization of the fast dynamics

Finding an analytical expression for the fast conductivities  $\mu(t)$  solutions of (1)-(3) cannot be done by directly solving the dynamics, because of the non-linear dependence on  $\mu(t)$  in the Laplacian pseudo-inverse. Nevertheless, here we propose an argument to characterize their long-time behavior, employing the dynamical system (10)-(11).

We support our findings with an empirical validation on synthetic networks built taking the Delaunay triangulation of  $|V|$  nodes placed at random in the square  $[0, 1] \times [0, 1]$ . In our experiments, we fixed  $|V| = 2^i$ , with  $i = 3, \dots, 9$ . The loads  $S(t)$  are set as  $S(t) := 20 S^1(t) + 10 S^4(t) + 5 S^8(t)$ , where each factor is defined as  $S^n(t) := q^n \cos(\omega n t)$ , with amplitudes extracted at random from a  $|V|$ -dimensional Dirichlet distribution as  $q^n \sim \text{Dir}(\alpha = 1) - 1/|V|$  (so that  $\sum_v S_v(t) = 0 \forall t \geq 0$ ), and  $n = 1, 4, 8$ . The period has been conventionally fixed so that  $\omega = 2\pi$ .

We observe that the evolution of the fast conductivities is typically divided in two phases, as shown in [Figure 2a](#). First, the conductivities undergo a stabilization phase for  $t < t_{\text{STAB}}$ , where they strongly depend on their initial conditions  $m_e$  and significantly change their mean values. Then, when  $t > t_{\text{STAB}}$ , the conductivities reach a plateau and oscillate around fixed values. More precisely, they either move around mean values that are far from zero, and preserve their oscillatory nature for all times, or they decay to zero with negligible oscillations that are progressively damped as  $t$  increases. These experimental observations suggest the following ansatz for the stabilized solutions  $\forall t > t_{\text{STAB}}$  and  $\forall e \in E$ :

$$\mu_e(t) = a_e + b_e(t) \quad \text{with } a_e = \text{const. and } b_e(t + T) = b_e(t). \quad (13)$$

We compare solutions of the new dynamics (10)-(11) with those of (1)-(3), see [Figure 2a](#) for an example of this comparison. In the figure the conductivities  $\mu(t)$  are oscillating around the values of  $\bar{\mu}(\tau)$  reached at convergence, that we denote with  $\bar{\mu}^\infty = \{\bar{\mu}_e^\infty\}_e$ . Motivated by this empirical observation, it is reasonable to set

$$a_e = \bar{\mu}_e^\infty \quad \forall e \in E. \quad (14)$$

We empirically notice that also the fluxes start to oscillate around a constant value after a first stabilization time interval (see [Figure 2a](#)), an evidence that we use to deduce (see [Appendix D](#)) that the main oscillatory modes of the conductivities are resonant with the *squared* fluxes, and have the form:

$$b_e(t) = \sum_{n,m \in \mathcal{N}} b_e^m b_e^n \exp(i\omega(n+m)t) \quad \forall e \in E, \quad (15)$$

with  $\mathcal{N} := \{n_v\}_v$  set of the Fourier modes of the loads. Hence, the conductivities oscillate with modes determined by those of the loads. This result is supported by several numerical experiments, see [Appendix D](#) for details.

Remarkably, these numerical experiments serve also as a validation for hypothesis (ii) in [Section 3.1](#), i.e. approximation (4). In fact, for any sufficiently slow time  $\tau$ , the conductivities fluctuate around a constant value, thus suggesting the possibility of neglecting their fast oscillatory nature when studying asymptotics of (1)-(3).

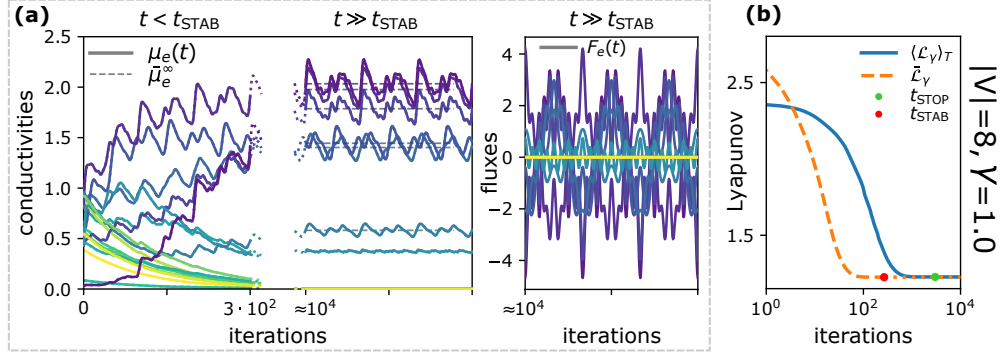


**Figure 2.** Characterization of the fast conductivities  $\mu(t)$ . All results are computed on a synthetic network with  $|V| = 8$ , and setting  $\gamma = 1.0$ . (a) Fast conductivities  $\mu(t)$  and fluxes  $F(t)$  are drawn with solid lines, stationary solutions  $\bar{\mu}^\infty$  are dashed. Labels on the  $x$ -axis correspond to the number of iterations of the numerical discretization of (1)-(3). Conductivities are depicted in two time windows, before and after their stabilization time,  $t_{\text{STAB}}$ . Fluxes are drawn only for  $t \gg t_{\text{STAB}}$ . Colors denote different edges. (b) Evolution of  $\bar{\mathcal{L}}_\gamma$  and of  $\langle \mathcal{L}_\gamma \rangle_T$  in time. The green and the red circles denote  $t_{\text{STOP}}$  and  $t_{\text{STAB}}$ .

#### 4.1. Candidate Lyapunov functional

We empirically observe (see Figure 2b) that our new dynamics (10)-(11) admits a candidate Lyapunov functional, i.e. a functional decreasing along solution trajectories, of the form

$$\bar{\mathcal{L}}_\gamma(\bar{\mu}) := \frac{1}{2} \sum_e \frac{\ell_e}{\bar{\mu}_e} \bar{F}_e^2(\bar{\mu}) + \frac{1}{2\gamma} \sum_e \ell_e \bar{\mu}_e^\gamma, \quad (16)$$

where for each edge  $e$ , we define  $\bar{F}_e^2 := (\bar{\mu}_e^2/\ell_e^2) \sum_{uv} A_{eu}(\bar{\mu}) A_{ev}(\bar{\mu}) C_{uv}$ . Noticeably, if  $\text{rank}(C) = 1$  holds, it is possible to formally prove that  $\bar{\mathcal{L}}_\gamma(\bar{\mu})$  is a well-defined Lyapunov for (10)-(11) (see Appendix C for detailed derivations). In addition, we can interpret the functional similarly to what done in [27] for multicommodity optimal transport. Namely, the Lyapunov is the sum of a dissipation cost, the first addend in (16), with an infrastructural cost—the price needed to build the transport network.

Empirically, we notice that the functional reaches a plateau at  $t_{\text{STOP}}$ , defined as the time for which  $\Delta \bar{\mathcal{L}}_\gamma / \delta t < \varepsilon$  is satisfied, with  $\Delta \bar{\mathcal{L}}_\gamma := |(\bar{\mathcal{L}}_\gamma)^{\tau+1} + (\bar{\mathcal{L}}_\gamma)^\tau| / (\bar{\mathcal{L}}_\gamma)^{\tau+1}$  and where the upper indexes denote consecutive iterations in the finite difference discretization of (10)-(11). In all our experiments, we choose  $\delta t = 0.1$  as time step of a Forward Euler method, and set the convergence threshold to  $\varepsilon = 10^{-5}$ .

Additionally, we observe that the candidate Lyapunov  $\bar{\mathcal{L}}_\gamma$  converges to a value that is the same achieved by the running average functional over the period  $T$ :

$$\langle \mathcal{L}_\gamma \rangle_T(t) := \frac{1}{T} \int_t^{t+T} \left( \frac{1}{2} \sum_v p_v(\mu) S(t') + \frac{1}{2\gamma} \sum_e \ell_e \mu_e^\gamma \right) dt' \quad (17)$$

with  $\mu$  that is evaluated along solution trajectories of (1)-(3). The functional (17) reaches a plateau at the stabilization time  $t_{\text{STAB}}$ , when the fast conductivities  $\mu(t)$  start oscillating around constant values. Remarkably, in Figure 2b we see that  $t_{\text{STAB}} \gg t_{\text{STOP}}$ , this is due to the fact that the time step  $\delta t$  for the numerical

discretization of (1)-(3) has to be set much lower than  $\bar{\delta}t$  in order to capture the oscillatory nature of the loads. In our experiments we set it to  $\delta t = \bar{\delta}t/10$ . A practical consequence of this is that the numerical discretization of (10)-(11) is a fast and scalable alternative to obtain the conductivities around which long-run solutions of (1)-(3) stabilize.

Because of this analogy between an optimal transport—functional minimization—setup and the solutions of our dynamical system, we can interpret the networks determined from the dynamics (10)-(11) as optimal topologies minimizing the infrastructural and dissipation cost. These topologies can also be achieved averaging long-run solutions of the original dynamics (1)-(3). In fact, as discussed in Section 4, long-run trajectories of (1)-(3) oscillate around asymptotics of the newly defined dynamical system (10)-(11).

## 5. Generation of loops

### 5.1. Conditions for the generation of loops in closed form

As mentioned, if  $C$  has  $\text{rank}(C) = 1$ , i.e.  $C_{uv} = y_u y_v$  for some  $y \in \mathbb{R}^{|V|}$ , the dynamics (10)-(11) produces trees at convergence. One trivial case where this holds is when the loads  $S(t)$  are static, i.e. constant for all times. However, this is not the only setting where  $\text{rank}(C) = 1$  is satisfied. In particular, there are cases where such condition holds but  $S$  do change in time. Here, we explore a case of study proposing an ansatz where the loads are the sum of decoupled harmonic oscillators:

$$S_v(t) = \sum_{i=1}^{N_v} A_v^i \cos(\omega n_v^i t + \phi_v^i) + d_v \quad \forall v \in V, \quad (18)$$

with  $\omega = 2\pi/T$ ,  $n_v^i, N_v \in \mathbb{N}$ , and  $A_v^i, d_v \in \mathbb{R}$ . By construction these loads are periodic in  $T$ , hence we compare them with their Fourier series representation  $S_v(t) = a_v^0/2 + \sum_{n_v \geq 1} a_v^{n_v} \cos(\omega n_v t + \varphi_v^{n_v})$ . Equating this expression with (18) yields:

$$c_v^{n_v} = \frac{A_v^i}{2} \exp(i\phi_v^i) \delta_{n_v n_v^i} \quad \forall n_v \in \mathbb{N}, \quad (19)$$

where we conventionally set  $\phi_v^0 = 0, \forall v \in V$ , and where only a finite number of Fourier coefficients are different from zero, given that the sum in (18) is finite.

The goal here is to express  $\text{rank}(C) = 1$  in terms of  $\{A_v^i\}$ ,  $\{n_v^i\}$ , and  $\{\phi_v^i\}$ , amplitudes, modes and phases of the harmonic oscillators. To do that, we start by noticing that  $\text{rank}(C) = 1$  is satisfied if and only if  $C_{uv} = y_u y_v, \forall u, v \in V$ , with  $y_v = \pm\sqrt{C_{vv}}$ , and where the plus or minus signs have to be determined among the  $2^{|V|}$  possible choices in such a way that  $\sum_v y_v = 0$  (see Appendix E for details).

Defining the complex vectors  $\nu_v = \{c_v^{n_v}\}^{n_v}$  with entries the Fourier coefficients in (19), we rewrite  $C_{uv} = \pm\sqrt{C_{uu}}\sqrt{C_{vv}}$  as  $\nu_u \cdot \nu_v = \pm\|\nu_u\|\|\nu_v\|$ , where the dot denotes the complex dot product, and  $\|\cdot\|$  is its correspondent norm. Thus, the rank condition on  $C$  can be reformulated in terms of an equivalent linear dependence condition of the form  $\nu_v = \lambda\nu_u$  between the vectors  $\nu_v, v \in V$ , and for  $\lambda \neq 0$ . Finally, substituting (19) in this linear dependence condition leads to the following main result.

**Proposition 1.** *Let the time-dependent loads  $S(t)$  injected in the network nodes be as in (18). If the following hold:*

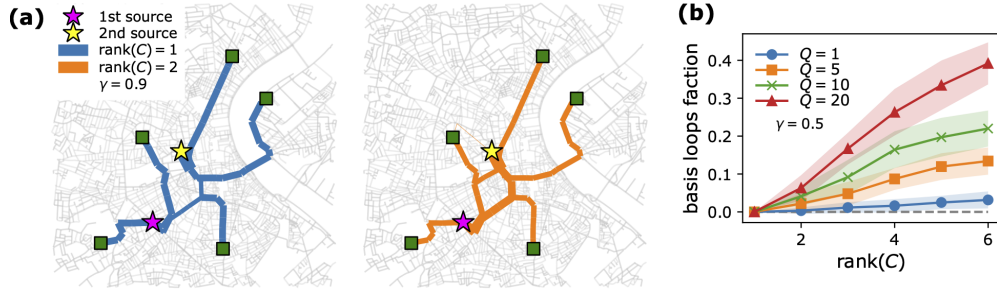


**Figure 3.** Bordeaux bus optimal transport network. (a) Network visualization. Input loads have been build as described in Section 5.2. The tree network originated by  $C$  with rank 1 is plotted in blue, the loopy topology in orange. The yellow and the magenta stars denote the geographical location of the two loads, the green square those of the sinks. Here width of edges correspond to slow conductivities at convergence,  $\bar{\mu}_e^\infty$ . Results are plotted for  $\gamma = 0.9$  (b) Basis loops fraction against  $\text{rank}(C)$ . Points correspond to averages over 100 runs of the experiments where positions of the sources and sinks are extracted at random. Shaded regions denote their standard deviations, results are plotted for  $\gamma = 0.5$ .

- (i)  $\phi_v^i = \phi_u^i + k\pi$ ,  $k \in \mathbb{Z}$ , i.e. sources and sinks are in phase,  
(ii)  $A_v^i \delta_{n_v n_v^i} = \lambda(-1)^k A_u^i \delta_{n_u n_u^i}$  (implying that that  $N_v = N$  for all  $v$ ),  
then, for any  $\gamma \leq 1$ , a stationary solution of (10)-(11) is a tree.

For a formal justification of this result see Appendix E.

### 5.2. Numerical tests on the Bordeaux bus

In order to test the rank condition on  $C$  we design two experiments on the real network of the buses of Bordeaux. The network topology has been constructed focusing on a central region of the city, and using data collected from [48]. Here, we assume that the loads, representing passengers entering or exiting the network, vary much faster than the conductivities. These latter quantities can be thought of as the size of the roads that a network manager needs to design, thus we can safely assume their evolution to happen on a larger time scale with respect to that of  $S(t)$ .

First, we design a simulation with two source nodes  $v_1, v_2$  (the stars in Figure 3a), and five sinks (the green squares in Figure 3a) that we extract at random among the nodes of the network. Then, we consider two cases where the sources are built in such a way that (i)  $\text{rank}(C) = 1$ , and (ii)  $\text{rank}(C) = 2$ . These are, respectively:

- (i)  $S_{v_1}(t) = S_{v_2}(t) = 100 \cos(\omega t)$ ,  $\omega = 2\pi$ ;  
(ii)  $S_{v_1}(t) = 100 \cos(\omega_1 t)$ ,  $\omega_1 = 2\pi$ , and  $S_{v_2} = 100 \cos(\omega_2 t)$ ,  $\omega_2 = 4\pi$ .

All the sinks  $u \neq v_1, v_2$  have loads  $S_u(t) = -(S_{v_1}(t) + S_{v_2}(t))/5$  in both cases, to ensure conservation of mass.

We expect that in the first case the network extracted from (10)-(11) with  $\gamma \leq 1$  is a tree. In the second case the network can possibly contain loops. We run the dynamics fixing  $\gamma = 0.9$  and we display our findings in Figure 3a. The empirical results reflect our predictions: the blue network—corresponding to the first case—is a tree. In contrast, in the orange network—second case—loops emerge.

We further validate our results on the bus network of Bordeaux with a second experiment. We assign the loads  $S_v(t) = \sum_{i=1}^n S_v^i(t)$ , with  $S_v^i = (100/|Q^n|) \cos(\omega_i t)$ ,

to a set  $Q^n$  of randomly extracted nodes, and  $S_v^i = -(100/(|V| - |Q^n|)) \cos(\omega it)$  to the remaining ones. The parameters are taken to be  $n = 1, \dots, 6$ , while the number of nodes which are randomly extracted for each  $n$  are  $Q := |Q^n| = \{1, 5, 10, 20\}$ . Here  $\omega = 2\pi$ . Exploiting the exact relation that the matrix  $C$  has with the modes of the loads (Section 5.1), it is possible to see that our particular construction of  $S(t)$  leads to  $1 \leq \text{rank}(C) \leq 6$ .

We show our results in Figure 3b, where we plot the fraction of basis loops of the network against the rank of matrix  $C$ . The dynamics is executed for  $\gamma = 0.5$  and the random extraction of the forcings has been changed for 100 runs. In the plot, it is clearly visible that for all values of  $Q$ , the fraction of basis loops is zero at  $\text{rank}(C) = 1$ . Moreover, we can see that when we increase the complexity to the problem, i.e. when  $\text{rank}(C)$  grows, the values attained on the  $y$ -axis increase. This suggests that the rank of the  $C$  can be used as a qualitative proxy to predict the number of loops in the optimal transport network. Lastly, as one could intuitively expect, the basis loops fraction increases with  $Q$ , i.e. with the number of nodes where mass is injected or extracted.

## 6. Conclusions

Routing models on networks are relevant to study many real-world problems. While most of the works in the current literature consider stationary setups, i.e. the inflows injected in the network do not change in time [2, 15, 20, 27, 37–42], few recent works investigate time-varying loads, and the majority of these models study solely the averaged evolution of the networks' variables [3, 9, 24, 37].

In this work, we analyze a dynamical systems where the conductivities—capacities of the network edges—are regulated by time-varying mass inflows. Motivated by biological observations [25, 43–45], we assume the existence of auxiliary conductivities that have response times which are much slower than those of the loads. Furthermore, in order to make the problem analytically tractable, we suppose that all the loads injected in nodes are periodic, in a period that substantially smaller than the adaptation time of the new conductivities. These two hypothesis together allow to deduce a dynamics where the evolution of the systems is solely regulated by an input matrix constructed using the Fourier series expansion of the loads.

The resulting dynamics allows to derive the main findings of our work. In detail, combining theoretical arguments with empirical evidence on synthetic networks, we find an expression for the long-run solutions of the original dynamics, that cannot otherwise simply be obtained solving the original dynamics. These long-run solutions are the sum of a stationary components, equal to the asymptotics of the dynamics we constructed, with an oscillatory one. This second contributions can be expressed as the sum of periodic signals, with modes related to those of the loads. Moreover, we discuss a sufficient condition on the loads that determines when optimal transport networks can be loop-less. Such condition is numerically validated on the Bordeaux bus network. Lastly, our dynamics can be connected to an optimization setup, as shown by the proposed candidate Lyapunov functional. As a result, asymptotic trajectories of our dynamics minimize the total cost needed to build the network infrastructure.

Importantly, the numerical discretization of the dynamics we proposed in this work can be used as an efficient method to rapidly converge to average long-run solutions of the original dynamics.

Our results can be extended in several ways. For instance, it would be interesting

to investigate different types of input loads that relax the periodicity hypothesis and use this to analyze the behaviour of the conductivities in different problems' settings. Similarly, it would be interesting to explore how this formalism adapts to multilayer networks, where passengers can enter in different stations corresponding to different transportation modes [20]. Another relevant application could be that of integrating our findings with the recent work of *Baptista et al.* [19], where the authors study how topological properties of the transport network change in time, as we approach stationary configurations, and how these reflect on the shape of the conductivities.

Altogether, we believe that our findings extend the current knowledge on network routing problems with time-varying input loads. To facilitate practitioners in using our model, we make the algorithmic implementation publicly available at <https://github.com/aleable/N-STARK>.

## 7. Acknowledgments

The authors thank the International Max Planck Research School for Intelligent Systems (IMPRS- IS) for supporting Alessandro Lonardi.

## Appendix A. Derivation of (5)

In order to introduce (5), we perform the following calculations on the right hand side of (2):

$$\int_{\tau}^{\tau+\Delta} \Phi_e(\mu(t), t) dt := \frac{1}{\Delta} \int_{\tau}^{\tau+\Delta} \mu_e^{-\gamma}(t) F_e^2(t) - \mu_e(t) dt \quad (\text{A.1})$$

$$= \frac{1}{\Delta} \int_{\tau}^{\tau+\Delta} \left( \frac{\mu_e^{2-\gamma}(t)}{\ell_e^2} \sum_{uvmn} B_{me} B_{ne} L_{um}^{\dagger}(\mu(t)) L_{vn}^{\dagger}(\mu(t)) S_u(t) S_v(t) - \mu_e(t) \right) dt \quad (\text{A.2})$$

$$\stackrel{t'=\tau+t}{=} \frac{1}{\Delta} \int_0^{\Delta} \left( \frac{\mu_e^{2-\gamma}(\tau+t')}{\ell_e^2} \sum_{uvmn} B_{me} B_{ne} L_{um}^{\dagger}(\mu(\tau+t')) L_{vn}^{\dagger}(\mu(\tau+t')) \times \right. \quad (\text{A.3})$$

$$\left. \times S_u(\tau+t') S_v(\tau+t') - \mu_e(\tau+t') \right) dt'$$

$$\stackrel{\text{(ii)}}{\approx} \frac{\mu_e^{2-\gamma}(\tau)}{\ell_e^2} \sum_{uv} A_{eu}(\mu(\tau)) A_{ev}(\mu(\tau)) \frac{1}{\Delta} \int_0^{\Delta} S_u(\tau+t') S_v(\tau+t') - \mu_e(\tau+t') dt' \quad (\text{A.4})$$

$$\stackrel{t=\tau+t'}{=} \frac{\mu_e^{2-\gamma}(\tau)}{\ell_e^2} \sum_{uv} A_{eu}(\mu(\tau)) A_{ev}(\mu(\tau)) \frac{1}{\Delta} \int_{\tau}^{\tau+\Delta} S_u(t) S_v(t) - \mu_e(t) dt \quad (\text{A.5})$$

$$=: \hat{\Phi}_e(\mu(\tau), \tau), \quad (\text{A.6})$$

which are valid  $\forall e \in E$ . In detail, in (A.2) we used the definition of the fluxes  $F_e(t) := \mu_e(t)(p_u(t) - p_v(t))/\ell_e, \forall e \in E$ , and evaluated the pressure solving Kirchhoff's law, i.e.  $p_v(t) := \sum_u L_{vu}^{\dagger}(\mu(t)) S_u(t), \forall v \in V$ . The second important step is in (A.4), where we used hypothesis (ii) in Section 3.1, namely approximation (4), to carry the conductivities out of the time integral, and we introduced  $A_{ev}(\mu(t)) := \sum_u B_{eu} L_{vu}^{\dagger}(\mu(t)), \forall e \in E, \forall v \in V$ .

## Appendix B. Derivation of (9)

We enforce the hypothesis of periodicity of the loads, i.e.  $S_v(t) = S_v(t + T)$ , with  $T/\Delta \ll 1$ , and we parametrize the integration window  $\Delta$  as  $\Delta = KT$ ,  $K \gg 1$ . This allows to split the integral in (9) into two separate contributions. In detail, making the reasonable hypothesis that  $S_u(t)S_v(t)$  is bounded by  $M < +\infty$ ,  $\forall t \geq 0$  and  $\forall u, v \in V$ , we can write:

$$\frac{1}{\Delta} \int_{\tau}^{\tau+\Delta} S_u(t)S_v(t) dt = \frac{1}{\Delta} \int_{\tau}^{\tau+\Delta} \sum_{n_u n_v} (c_u^{n_u})^* c_v^{n_v} \exp(i\omega(n_v - n_u)t) dt \quad (\text{B.1})$$

$$= \sum_{n_u n_v} (c_u^{n_u})^* c_v^{n_v} \left( \sum_{k=1}^{\lfloor K \rfloor} \mathcal{I}_k(n_u, n_v) + \mathcal{I}_K(n_u, n_v) \right) \quad (\text{B.2})$$

with:

$$\mathcal{I}_k(n_u, n_v) = \frac{1}{\Delta} \int_{\tau+(k-1)T}^{\tau+kT} \exp(i\omega(n_v - n_u)t) dt \quad \forall k = 1, \dots, \lfloor K \rfloor, \quad (\text{B.3})$$

$$\mathcal{I}_K(n_u, n_v) = \frac{1}{\Delta} \int_{\tau+\lfloor K \rfloor T}^{\tau+KT} \exp(i\omega(n_v - n_u)t) dt. \quad (\text{B.4})$$

Hence, we separate the first  $\lfloor K \rfloor$  integrals over the period  $T$  and the last one in  $(\lfloor K \rfloor T, KT)$ . Since  $K \gg 1$ , the first  $\lfloor K \rfloor$  contributions can be evaluated as

$$\sum_{n_u n_v} (c_u^{n_u})^* c_v^{n_v} \sum_{k=1}^{\lfloor K \rfloor} \mathcal{I}_k(n_u, n_v) = \frac{\lfloor K \rfloor}{K} \sum_{n_u n_v} (c_u^{n_u})^* c_v^{n_v} \delta_{n_u n_v} \quad (\text{B.5})$$

$$= \sum_{n_v} (c_u^{n_v})^* c_v^{n_v} + \mathcal{O}(\Delta), \quad (\text{B.6})$$

with  $\delta_{ij}$  being Kronecker delta for two indices  $i, j$ . As for the second term, in the limit  $K \gg 1$  we can write

$$\left| \sum_{n_u n_v} (c_u^{n_u})^* c_v^{n_v} \mathcal{I}_K(n_u, n_v) \right| \leq \frac{K - \lfloor K \rfloor}{K} M \sim \mathcal{O}(\Delta), \quad (\text{B.7})$$

showing that integrals over the small interval  $(\lfloor K \rfloor T, KT)$  are negligible for a large integration window.

## Appendix C. Sufficient rank condition for optimal trees

We discuss in detail the sufficient condition  $\text{rank}(C) = 1$  to obtain loop-less optimal networks running the dynamics (10)-(11). Our argument proceed as follows.

The matrix  $C$  is symmetric by construction, thus if its rank is 1 its eigenvalue decomposition is of the form  $C = \sum_{i=1}^N \lambda_i x_i x_i^\top$ , with all the eigenvalues equal to zero except one. We conventionally choose it to be  $\lambda_1 = \sum_v C_{vv} > 0$ , with a unit norm eigenvector  $x_1$ . Defining  $y := \sqrt{\lambda_1} x_1$  and substituting the eigendecomposition of  $C$  in (12) we get that  $\bar{\Phi}_e$  is proportional to  $\hat{F}_e := (\bar{\mu}_e/\ell_e) \sum_v B_{ev} \hat{p}_v$ , with  $\hat{p}_v := \sum_u L_{vu}^\dagger(\bar{\mu}) y_u$ . In order to conclude, we need to show that  $\hat{p}$  is a well-defined

solution of Kirchhoff's law,  $\sum_u L_{uv}(\bar{\mu})\hat{p}_u = y_v$ , i.e.  $y$  is a zero-sum vector [47]. This comes as a consequence of conservation of mass. Indeed, since for all times  $\sum_v S_v(t) = 0$  holds, we have  $\sum_v S_u(t)S_v(t) = 0, \forall u \in V$ . Using (9) and ignoring negligible terms of order  $\mathcal{O}(\Delta)$ , this yields  $\sum_v C_{uv} = 0, \forall u \in V$ . Finally, substituting the eigendecomposition of  $C$  in this last relation gives  $\sum_v y_u y_v = 0, \forall u \in V$ . This is satisfied only if  $\sum_v y_v = 0$ , i.e.,  $y$  is a zero-sum vector. In this case, (10)-(11) corresponds to the standard dynamics (1)-(3) with constant loads, which are  $S(t) = y, \forall t \geq 0$ , and we recover the well-know result that optimal networks are trees for  $\gamma \leq 1$  [23, 26, 29].

*Rank 1 condition and Lyapunov functional.* Noticeably, if  $\text{rank}(C) = 1$ , it is possible to prove that the functional  $\tilde{\mathcal{L}}_\gamma(\bar{\mu})$  proposed in (16) is a well-defined Lyapunov functional. This means that for any  $\bar{\mu}(\tau)$  solution trajectory of (10)-(11), we have  $d\tilde{\mathcal{L}}_\gamma(\bar{\mu}(\tau))/d\tau \leq 0$ , with stationarity achieved only by asymptotics of the dynamics. Having established that  $\hat{p}$  is a well-defined potential, we can in write the Lyapunov functional as  $\tilde{\mathcal{L}}_\gamma(\bar{\mu}) = (1/2)\sum_v \hat{p}_v(\bar{\mu})S_v + (1/2\gamma)\sum_e \ell_e \bar{\mu}_e^\gamma$ . This last expression is useful to conclude the proof, as shown in [27].

#### Appendix D. Derivation of (15)

In order to discern the nature of fast oscillating component  $b_e(t)$  of the stabilized solutions, we need to investigate further the original dynamics (1)-(3). From our numerical validation we observe that the fluxes start to oscillate around a constant value after a first stabilization time interval (see Figure 2a), analogously to the conductivities. This suggest the ansatz  $F_e(t) = \sum_{n_e \in \mathbb{Z}} F_e^{n_e} \exp(i\omega n_e t), \forall e \in E$ , for all times  $t$  sufficiently larger than  $t_{\text{STAB}}$ , and with the terms  $F_e^{n_e}$  amplitudes of the Fourier series decomposition. We argue that pairing this expression with Kirchhoff's law, i.e.  $\sum_e B_{ve}F_e(t) = S_v(t)$ , yields

$$F_e(t) = \sum_{n \in \mathcal{N}} F_e^n \exp(i\omega n t) \quad \forall e \in E, \quad (\text{D.1})$$

with  $\mathcal{N} := \{n_v\}_v$ , with  $\mathcal{N} := \{n_v\}_v$  set of Fourier modes of the loads injected in the network. Our argument is the following.

Assuming the ansatz  $F_e(t) = \sum_{n_e \in \mathbb{Z}} F_e^{n_e} \exp(i\omega n_e t), \forall e \in E$ , we separate the contributions:

$$F_e(t) = \varphi_e(t) + \psi_e(t) \quad (\text{D.2})$$

$$\varphi_e(t) = \sum_{n_e \in \mathcal{N}} F_e^{n_e} \exp(i\omega n_e t) \quad (\text{D.3})$$

$$\psi_e(t) = \sum_{n_e \notin \mathcal{N}} F_e^{n_e} \exp(i\omega n_e t). \quad (\text{D.4})$$

Substituting (D.2)-(D.4) in Kirchhoff's law returns the conditions:

$$\sum_e B_{ve}\varphi_e(t) = S_v(t) \quad (\text{D.5})$$

$$\sum_e B_{ve}\psi_e(t) = 0, \quad (\text{D.6})$$

valid  $\forall v \in V$ . Now, in order to guarantee that the fluxes  $\{\varphi_e(t), \psi_e(t)\}$  are well-defined, we suppose the existence of two time-dependent potentials:  $\alpha(t) = \{\alpha_v(t)\}_v$  and  $\beta(t) = \{\beta_v(t)\}_v$ . These are defined on the network nodes and such that  $\forall e \in E$  we have

$$\varphi_e(t) := \frac{\mu_e}{\ell_e} \sum_v B_{ve} \alpha_v(t) \quad (\text{D.7})$$

$$\psi_e(t) := \frac{\mu_e}{\ell_e} \sum_v B_{ve} \beta_v(t). \quad (\text{D.8})$$

These definitions are consistent with that of  $F_e(t)$  being a potential-based flux, and yield  $p_v(t) = \alpha_v(t) + \beta_v(t), \forall v \in V$ . Substituting (D.7) and (D.8) in (D.5) and (D.6) respectively, implies that  $\psi_e(t) = 0, \forall e \in E$ , and for sufficiently large times. Hence, the only non-zero terms in the Fourier decomposition of  $F_e(t)$  have modes in  $\mathcal{N}$ .

This result is particularly useful to describe the behavior of  $\mu(t)$  at large times. First, we recall that  $\mu_e(t) = \bar{\mu}_e^\infty + b_e(t), \forall e \in E$ , as discussed in Section 4. Moreover, we observe that in our numerical experiments (see Figure 2a) the size of the amplitude of the oscillatory term  $b_e(t)$  is negligible in size with respect to  $\bar{\mu}_e^\infty$ , unless  $\mu_e(t)$  decays to zeros. This allows to approximate (2) as

$$\frac{d\mu_e(t)}{dt} \simeq \frac{F_e^2(t)}{(\bar{\mu}_e^\infty)^\gamma} - \mu_e(t) \quad \forall e \in E. \quad (\text{D.9})$$

Finally, substituting (D.1) in (D.9), we get the desired results, i.e., the main oscillatory modes of the conductivities, hence of  $b_e(t)$ , are resonant with the squared fluxes. Thus we obtain (15).

*Numerical validation on synthetic networks.* We test these expressions numerically on networks generated as described in Section 4. We compute  $P_e := \int_{\mathbb{R}} |\mathcal{F}[b_e](f)|^2 df$ , the total spectral density of the oscillatory components  $b_e(t)$ , after the conductivities  $\mu(t)$  stabilize. Here  $\mathcal{F}[\cdot](f)$  is the Fourier transform operator. Additionally, we calculate  $P_{\mathcal{N}}$ , obtained summing the atomic contributions of the spectral density on the modes  $k \in \mathcal{K} := \{k | k = n + m, \text{ for } n, m \in \mathcal{N}\}$ . Namely,  $P_{\mathcal{N},e} := \sum_{k \in \mathcal{K}} \int_{\mathbb{R}} |\mathcal{F}[b_e](f)|^2 \delta(f - k) df, \forall e \in E$ .

From (15), we expect to have most of the spectral density of  $b_e(t)$  concentrated on the modes in  $\mathcal{K}$ , i.e. the ratio  $P_e/P_{\mathcal{N},e}$  should be close to 1 for each edge. In Figure D1a we plot  $P = \{P_e\}_e$  versus  $P_{\mathcal{N}} = \{P_{\mathcal{N},e}\}_e$  for the example network considered in Figure 2. The plot supports (15), indeed the element-wise ratio  $P/P_{\mathcal{N}}$  is close to 1 for all points (each correspondent to a different edge) with a slight deviation only for small (thus negligible) values of the conductivities. We further validated this result on an additional synthetic example network. We constructed the Delaunay networks described in Section 4 considering 100 combinations of seeds for the nodes' positions and for the random input loads. Then, we computed the spectral densities,  $P$ , and plotted them against  $\delta P$ , with entries  $\delta P_e := (P_{\mathcal{N},e} - P_e)/P_e$ . We show in Figure D1b results for  $\gamma = 0.5, 1, 1.5$  and on 100 random graphs of size  $|V| = 8$ . Here, we clearly see that  $\delta P$  are negligible for any edge with  $P$  larger than a threshold  $\alpha$  (in our experiments we fix  $\alpha = 10^{-3}$ ), further validating the result supported by Figure D1a.

It is worth mentioning how the points cluster in different regions of the plot, for different values of  $\gamma$ . The green points, corresponding to  $\gamma = 0.5$ , are divided in two clusters: one around  $P$  small and  $\delta P = 1$ , and another with  $P$  large and  $\delta P$  negligible.

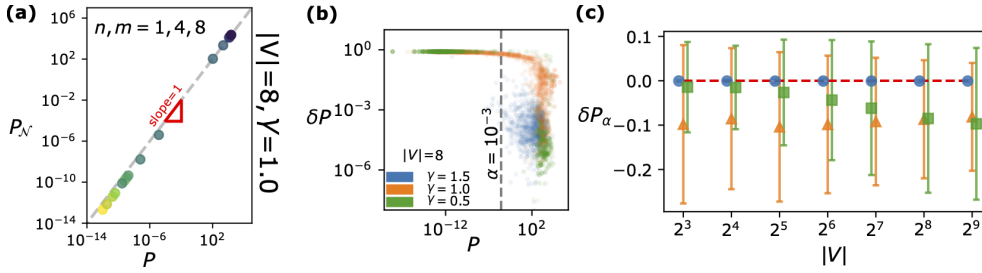


**Figure D1.** Spectral density validation. (a)  $P_N$  versus  $P$  for the example network of Figure 2. Each point, drawn with a different color, corresponds to an edge, the color scale is that of Figure 2a. (b)  $P$  versus  $\delta P$ . Each point corresponds to an edge, marker color denotes  $\gamma = 0.5, 1, 1.5$ . The dashed line is the cut-off used to build  $\delta P_\alpha$ . (c) Compatibility of  $\delta P_\alpha$  with  $\delta P_\alpha = 0$  for different networks' sizes. Markers and bars correspond to averages and standard deviations computed over 100 random configurations of the problem. The networks have been obtained pairing 10 seeds for nodes coordinates generation and 10 seeds for random mass and conductivities initialization,  $\mu_e \sim \text{Unif}(0, 1)$ .

This reflects the tendency of  $\gamma < 0.5$  to aggregate fluxes on few edges. The blue points, corresponding to  $\gamma = 1.5$ , are instead concentrated around a region with  $P$  large and  $\delta P$  small, since in this case fluxes are distributed on more edges. Finally, the orange points, corresponding to  $\gamma = 1$ , represent a transition between the two cases, and are located in a cluster placed in between the other two. This result is consistent with the behavior of  $\gamma$  mentioned in Section 2.

We test the scalability of our result by running the same validation just described, but increasing the graphs sizes. We plot our results in Figure D1c. Here we show the compatibility of  $\delta P_\alpha := \sum_e \delta P_e \mathbb{I}(\delta P_e > \alpha) / E'$  with zero. Here  $\mathbb{I}(\cdot)$  is the indicator function, and  $E'$  the number of the edges that do not get trimmed by  $\alpha$ . We see that all values attain values close to  $\delta P_\alpha = 0$ , and all errorbars (expressing standard deviations over 100 random graph realizations) are always intersecting the line highlighting  $\delta P_\alpha = 0$ . The decreasing trend of  $\delta P_\alpha$  for  $\gamma = 0.5$  can be attributed to the fact that we fixed the cut-off threshold  $\alpha$  a priori, and thus we do not have a precise trim for  $P$  for larger networks.

## Appendix E. Harmonic oscillator conditions

*Rank 1 and product of diagonal entries of  $C$ .* We already established that if  $\text{rank}(C) = 1$ , then there exists a zero-sum vector  $y$  such that  $C_{uv} = y_u y_v, \forall u, v \in V$  (see Appendix C). Inspecting the diagonal elements of  $C$ , it is immediate to get  $y_v = \pm \sqrt{C_{vv}}, \forall v \in V$ . Here, the choice of the plus or minus signs is constrained among the  $2^{|V|}$  possibilities, to those for which  $\sum_v y_v = 0$  holds. The right-to-left implication comes naturally from the definition of  $C$ . Namely, if we suppose that  $C_{uv} = y_u y_v, \forall u, v \in V$ , we are imposing that all the columns of  $C$  are scalar multipliers of each other, i.e.  $\text{rank}(C) = 1$ .

*Conditions on the harmonic oscillators' parameters.* Substituting (19) in  $\nu_v = \lambda \nu_u$ , leads to

$$A_v^i \exp(i\phi_v^i) \delta_{n_v n_v^i} = \lambda A_u^i \exp(i\phi_u^i) \delta_{n_u n_u^i}, \quad (\text{E.1})$$

which needs to be satisfied for each pair of  $n_u, n_v \in \mathbb{N}$ . This is valid if the phases are such that  $\phi_v^i = \phi_u^i + k\pi$ ,  $k \in \mathbb{Z}$ , i.e. condition (i) in Section 5.1 holds. Substituting this last equality in (E.1), we get

$$A_v^i \exp(i\phi_v^i) \delta_{n_v n_v^i} = \lambda A_u^i \exp(i\phi_u^i) (-1)^k \delta_{n_u n_u^i} \quad (\text{E.2})$$

$$A_v^i \delta_{n_v n_v^i} = \lambda A_u^i (-1)^k \delta_{n_u n_u^i}, \quad (\text{E.3})$$

that is precisely (ii) in Section 5.1. In conclusion, fixing the input loads in such a way that (i) and (ii) hold lead to  $\text{rank}(C) = 1$ , which is sufficient to get optimal tree topologies, as shown in Appendix C.

## References

- [1] Ronellenfitch H and Katifori E 2016 *Phys. Rev. Lett.* **117**(13) 138301 URL <https://link.aps.org/doi/10.1103/PhysRevLett.117.138301>
- [2] Ronellenfitch H and Katifori E 2019 *Phys. Rev. Lett.* **123**(24) 248101 URL <https://link.aps.org/doi/10.1103/PhysRevLett.123.248101>
- [3] Katifori E, Szöllösi G J and Magnasco M O 2010 *Phys. Rev. Lett.* **104**(4) 048704 URL <https://link.aps.org/doi/10.1103/PhysRevLett.104.048704>
- [4] Xia Q 2007 *ESAIM: Control, Optimisation and Calculus of Variations* **13** 359–377 URL <http://www.numdam.org/articles/10.1051/cocv:2007016/>
- [5] Sinclair K and Ball R C 1996 *Phys. Rev. Lett.* **76**(18) 3360–3363 URL <https://link.aps.org/doi/10.1103/PhysRevLett.76.3360>
- [6] Rinaldo A, Rodriguez-Iturbe I, Rigon R, Bras R L, Ijjasz-Vasquez E and Marani A 1992 *Water Resources Research* **28** 2183–2195 URL <https://agupubs.onlinelibrary.wiley.com/doi/abs/10.1029/92WR00801>
- [7] Rinaldo A, Rodriguez-Iturbe I, Rigon R, Ijjasz-Vasquez E and Bras R L 1993 *Phys. Rev. Lett.* **70**(6) 822–825 URL <https://link.aps.org/doi/10.1103/PhysRevLett.70.822>
- [8] Sun T, Meakin P and Jøssang T 1994 *Phys. Rev. E* **49**(6) 4865–4872 URL <https://link.aps.org/doi/10.1103/PhysRevE.49.4865>
- [9] Konkol A, Schwenk J, Katifori E and Shaw J B 2021 Interplay of river and tidal forcings promotes loops in coastal channel networks (*Preprint* [2108.04151](https://arxiv.org/abs/2108.04151))
- [10] Tero A, Takagi S, Saigusa T, Ito K, Bebbler D P, Fricker M D, Yumiki K, Kobayashi R and Nakagaki T 2010 *Science* **327** 439–442 ISSN 0036-8075 URL <https://science.sciencemag.org/content/327/5964/439>
- [11] Tero A, Yumiki K, Kobayashi R, Saigusa T and Nakagaki T 2008 *Theory in biosciences* **127** 89–94 URL <https://doi.org/10.1007/s12064-008-0037-9>
- [12] Tero A, Kobayashi R and Nakagaki T 2006 *Physica A: Statistical Mechanics and its Applications* **363** 115–119 ISSN 0378-4371 information and Material Flows in Complex Networks URL <https://www.sciencedirect.com/science/article/pii/S0378437106000963>
- [13] Tero A, Kobayashi R and Nakagaki T 2007 *Journal of Theoretical Biology* **244** 553–564 ISSN 0022-5193 URL <https://www.sciencedirect.com/science/article/pii/S002251930600289X>
- [14] Yamada H, Toth A and Nakagaki T 2000 *Nature* **407** 470–470 URL <https://doi.org/10.1038/35035159>
- [15] Bonifaci V 2013 *Information Processing Letters* **113** 4–7 ISSN 0020-0190 URL <https://www.sciencedirect.com/science/article/pii/S0020019012002621>
- [16] Bonifaci V 2017 *Journal of mathematical biology* **74** 567–581 URL <https://doi.org/10.1007/s00285-016-1036-y>
- [17] Baptista D, Leite D, Facca E, Putti M and De Bacco C 2020 *Scientific Reports* **10**(1) 088702 URL <https://doi.org/10.1038/s41598-020-77064-4>
- [18] Baptista D and De Bacco C 2021 *R. Soc. open sci.* **8** 210025 URL <http://doi.org/10.1098/rsos.210025>
- [19] Baptista D and Bacco C D 2021 Convergence properties of optimal transport-based temporal networks (*Preprint* [2109.00971](https://arxiv.org/abs/2109.00971))
- [20] Ibrahim A A, Lonardi A and De Bacco C 2021 *Algorithms* **14** URL <https://doi.org/10.3390/a14070189>
- [21] Bonifaci V, Facca E, Folz F, Karrenbauer A, Kolev P, Mehlhorn K, Morigi G, Shahkarami G and Vermande Q 2021 Physarum Multi-Commodity Flow Dynamics (*Preprint* [2009.01498](https://arxiv.org/abs/2009.01498))

- [22] Yeung C H, Saad D and Wong K Y M 2013 *Proceedings of the National Academy of Sciences* **110** 13717–13722 ISSN 0027-8424 URL <https://www.pnas.org/content/110/34/13717>
- [23] Bohn S and Magnasco M O 2007 *Phys. Rev. Lett.* **98**(8) 088702 URL <https://link.aps.org/doi/10.1103/PhysRevLett.98.088702>
- [24] Corson F 2010 *Phys. Rev. Lett.* **104**(4) 048703 URL <https://link.aps.org/doi/10.1103/PhysRevLett.104.048703>
- [25] Hu D, Cai D and Rangan A V 2012 *PLoS ONE* **7** 1–13 URL <https://doi.org/10.1371/journal.pone.0045444>
- [26] Kirkegaard J B and Sneppen K 2020 *Phys. Rev. Lett.* **124**(20) 208101 URL <https://link.aps.org/doi/10.1103/PhysRevLett.124.208101>
- [27] Lonardi A, Facca E, Putti M and De Bacco C 2021 *Phys. Rev. Research* **3**(4) 043010 URL <https://link.aps.org/doi/10.1103/PhysRevResearch.3.043010>
- [28] Lonardi A, Putti M and De Bacco C 2021 *arXiv preprint arXiv:2110.06171*
- [29] Banavar J R, Colaioni F, Flammini A, Maritan A and Rinaldo A 2000 *Phys. Rev. Lett.* **84**(20) 4745–4748 URL <https://link.aps.org/doi/10.1103/PhysRevLett.84.4745>
- [30] Xia Q 2003 *Communications in Contemporary Mathematics* **5** 251–279
- [31] Mezard M and Montanari A 2009 *Information, physics, and computation* (Oxford University Press)
- [32] Yeung C H and Saad D 2012 *Phys. Rev. Lett.* **108**(20) 208701 URL <https://link.aps.org/doi/10.1103/PhysRevLett.108.208701>
- [33] Yeung C H and Saad D 2011 *Journal of Physics A Mathematical and Theoretical* **46** 103001 URL <https://iopscience.iop.org/article/10.1088/1751-8113/46/10/103001>
- [34] Altarelli F, Braunstein A, Dall’Asta L, De Bacco C and Franz S 2016 *PLOS ONE* **10** 1–18 URL <https://doi.org/10.1371/journal.pone.0145222>
- [35] Bacco C D, Franz S, Saad D and Yeung C H 2014 *Journal of Statistical Mechanics: Theory and Experiment* **2014** P07009 URL <https://doi.org/10.1088/1742-5468/2014/07/p07009>
- [36] Xu Y Z, Po H F, Yeung C H and Saad D 2021 Scalable node-disjoint and edge-disjoint multi-wavelength routing (*Preprint 2107.00609*)
- [37] Hu D and Cai D 2013 *Phys. Rev. Lett.* **111**(13) 138701 URL <https://link.aps.org/doi/10.1103/PhysRevLett.111.138701>
- [38] Bonifaci V, Mehlhorn K and Varma G 2012 *Journal of Theoretical Biology* **309** 121 – 133 ISSN 0022-5193 URL <http://www.sciencedirect.com/science/article/pii/S0022519312003049>
- [39] Facca E, Cardin F and Putti M 2016 *SIAM Journal on Applied Mathematics* **78** 651–676 URL <https://doi.org/10.1137/16M1098383>
- [40] Facca E, Daneri S, Cardin F and Putti M 2020 *Journal of Scientific Computing* **82** 68 URL <https://link.springer.com/article/10.1007/s10915-020-01170-8>
- [41] Facca E, Cardin F and Putti M 2021 *Journal of Computational Physics* **447** 110700 ISSN 0021-9991 URL <https://www.sciencedirect.com/science/article/pii/S0021999121005957>
- [42] Facca E, Cardin F and Putti M 2020 Physarum Dynamics and Optimal Transport for Basis Pursuit (*Preprint 1812.11782*)
- [43] Folkow B, Lundgren O and Wallentin I 1963 *Acta physiologica scandinavica* **57** 270–283
- [44] Granger D N, Kvietys P R and Perry M A 1982 *American Journal of Physiology-Gastrointestinal and Liver Physiology* **242** G570–G574
- [45] Widmer R J, Stewart R H, Young M F, Laurinec J E, Laine G A and Quick C M 2007 *American Journal of Physiology-Regulatory, Integrative and Comparative Physiology* **292** R2312–R2317 URL <https://doi.org/10.1152/ajpregu.00873.2006>
- [46] “Transport for London open data”, accessed: 2021-09-20 (2021)
- [47] Klein D J and Randić M 1993 *Journal of Mathematical Chemistry* **12**(1) URL <https://doi.org/10.1007/BF01164627>
- [48] Kujala R, Weckström C, Darst R K, Mladenović M N and Saramäki J 2018 *Scientific data* **5** 180089 URL <https://doi.org/10.1038/sdata.2018.89>